A CubeSat Add-On for Resolving Phase Unwrapping Errors in Single-Pass SAR Interferometry

Maxwell Nogueira Peixoto, Michelangelo Villano
German Aerospace Center (DLR), Microwaves and Radar Institute, Germany

Abstract

Digital elevation models can be obtained from synthetic aperture radar (SAR) interferograms though the process of phase unwrapping. Even with high-quality bistatic interferograms, such as those produced by TanDEM-X, however, unwrapping errors occur, which are usually resolved by exploiting an additional acquisition over the same scene with a shorter baseline. This work proposes to upgrade a bistatic interferometric SAR system with a low-cost CubeSat add-on that allows detecting and resolving phase unwrapping errors in a single pass of the satellites. Simulation analyses show the effectiveness of the CubeSat add-on in spite of its much smaller antenna aperture.

1 Introduction

Synthetic aperture radar (SAR) is a class of active coherent radars particularly suitable for satellite remote sensing. SAR interferometry is a technique where two SAR images taken over the same area with temporal or spatial separation, called the baseline, are combined into an interferogram from which information can be extracted. An important application of SAR interferometry is the generation of accurate high-resolution digital elevation models (DEMs). For such, an across-track baseline must be present, so that the interferometric phase is related to the height of the imaged cell, with a 2π phase variation corresponding to the variation in height equal to the so called height of ambiguity. Additionally, acquiring both SAR images in a single-pass configuration avoids temporal decorrelation [1]-[4]. Spaceborne single-pass SAR interferometry was demonstrated by the Shuttle Radar Topography Mission (SRTM), and later by the TanDEM-X mission, where two TerraSAR-X-like satellites fly in close formation. Both these missions achieved the goal of producing the most accurate global-scale digital elevation model of their time [5], [6].

Phase unwrapping is a critical step in generating a DEM from an interferogram, and even with SAR instruments in a single-pass configuration, such as in TanDEM-X, phase unwrapping errors may occur [7]. The information from an additional interferogram acquired over the same area but with a different height of ambiguity can be used to resolve phase unwrapping errors. TanDEM-X uses this approach, with the additional interferogram being obtained in a second pass of the satellites [7], which requires adapting the formation to the new baseline, impacts the acquisition plan of the mission, and limits the system's capability of monitoring fast-changing dynamic phenomena. This work proposes instead that the additional interferogram is obtained in a single pass through a low-cost, receive-only CubeSat add-on flying in close formation with the bistatic interferometer. The CubeSat add-on is characterized by an antenna aperture much smaller than that of the main two satellites. This work describes and analyses this concept and presents some design examples for the case where a CubeSat is added to a TanDEM-X-like interferometer.

2 Bistatic SAR Interferometry with a CubeSat Add-On

We propose an interferometric SAR system concept where a bistatic SAR interferometer is augmented with one or two receive-only CubeSat SARs that provide information for detecting and resolving phase unwrapping errors. Two configurations are considered. In the first, shown in Figure 1 (a), a single CubeSat is added with a small baseline to one of the main satellites. As maintaining this small baseline in close formation flight may be challenging, the second configuration, shown in Figure 1 (b), is proposed where two CubeSats are added with a small baseline between themselves, and an along-track separation from the main satellites. One of the main satellites is responsible for transmitting the pulses that illuminate the scene, and all satellites record the echoes. Three interferograms are formed by combining the coregistered images from each satellite. The large-baseline interferogram, v_L, is formed with the main satellites, and has a large baseline to provide precision to the resulting DEM. In contrast, a small-baseline interferogram, v_S, is formed, in the first configuration, from the CubeSat and one of the main satellites, and, in the second configuration, from the two CubeSats. Its small baseline leads to a large height of ambiguity, which enables it to be used to resolve phase unwrapping errors. A third interferogram called the medium-baseline interferogram can be formed, in the first configuration, by combining the images of the CubeSat and the other main satellite or, in the second configuration, by combining the large-baseline and the small-baseline interferograms through

$$v_M = v_L v_S^*. \tag{1}$$

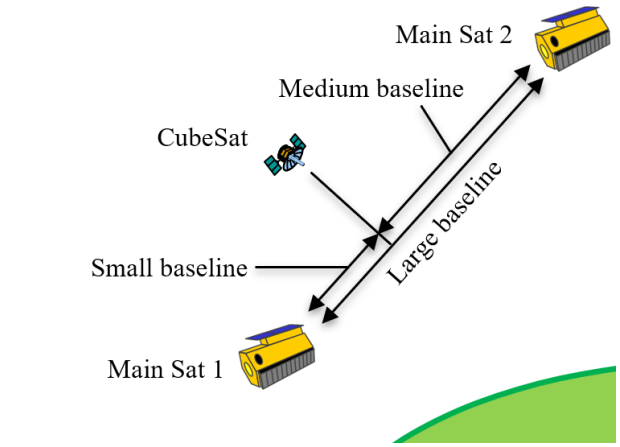

(a)

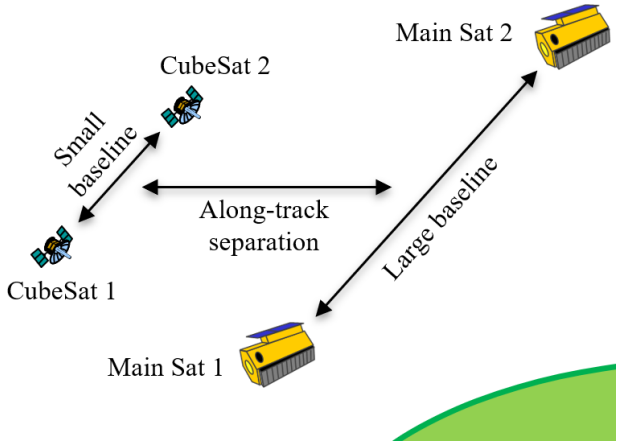

(b)

Figure 1 Diagram showing the two proposed configurations for the CubeSat add-on to a bistatic SAR interferometer. In the first (a), a CubeSat is added in formation with a small baseline to one of the main satellites. In the second (b), two CubeSats are added with a small baseline between themselves and an along-track separation from the main interferometer.

To leverage the additional information provided by the CubeSat add-on, a multi-baseline phase unwrapping algorithm can be used. In this work, we propose a processing concept based on the dual-baseline phase unwrapping framework for TanDEM-X [7]. As shown in Figure 2, the phases of the three interferograms are unwrapped independently and converted to heights, forming three DEMs. The large-baseline DEM height h_L is corrected by adding or subtracting a multiple of the height of ambiguity that minimizes the difference with the small-baseline DEM height h_S:

$$h_{\text{final}} = h_L + \left\lfloor \frac{h_S - h_L}{HoA_L} \right\rceil HoA_L, \qquad (2)$$

where $\lfloor \cdot \rceil$ denotes rounding to the nearest integer, HoA_L is the height of ambiguity of the large-baseline DEM, and h_{final} is the corrected height. This correction is done pixelwise. With this method, the resolution and height variance of the final DEM are the same as that of the large-baseline DEM.

The error in the height of the small-baseline DEM with respect to the true height of the terrain can cause residual unwrapping errors to be present, i.e., cause the unwrapping correction procedure to add or subtract an incorrect number of heights of ambiguity, such that the final height h_{final} contains unwrapping errors. These errors are attributed to the large height variance of the small-baseline DEM due to its large height of ambiguity and lower coherence, and to biases in the small-baseline DEM such as unwrapping errors or the effect of strong coherent azimuth ambiguities [8]. Because phase unwrapping errors generally occur in large blobs, it is acceptable to trade the resolution of the small-baseline DEM to further reduce unwrapping errors or reduce the downlink data volume. One possibility is to increase the number of looks used in the small-baseline interferogram, reducing the height variance of the small-baseline DEM and, therefore, decreasing the likelihood of residual unwrapping errors. Another possibility is receiving a smaller range bandwidth in the CubeSat, which would also reduce the data volume to be downlinked.

Phase unwrapping errors are detected by comparison of the large-baseline DEM with the medium- and small-baseline DEMs and, to avoid residual unwrapping errors from being introduced into the final DEM, this information is used to skip the phase unwrapping correction described in (2) in the regions where phase unwrapping errors are not detected. If the difference between the heights of the large-baseline and medium-baseline DEMs, h_L and h_M, respectively, is larger than the difference between the corresponding heights of ambiguity, HoA_L and HoA_M, i.e., if

$$|h_L - h_M| > |HoA_L - HoA_M|, \qquad (3)$$

the heights are considered discrepant, revealing the presence of unwrapping errors, and the phase unwrapping correction (2) is performed. This check is evaluated pixelwise and can fail to detect the unwrapping errors if the offsets caused by them in the large- and medium-baseline DEMs do not differ by much more than the threshold in (3). To avoid this, with respect to the original phase unwrapping approach of TanDEM-X, we propose to further compare the heights of large-baseline DEM with those of the small-baseline DEM, such that if they differ by more than some predefined threshold, the heights are considered discrepant and the phase unwrapping correction (2) is performed. The recommended value for the threshold is 1.5 times the height of ambiguity of the large-baseline DEM as a height difference exceeding it would cause the phase unwrapping correction in (2) to add or subtract two or more heights of ambiguity to the large-baseline DEM. We additionally propose to smooth this mask of unwrapping error detections by blurring then thresholding, or by using an algorithm such as DBSCAN [9] and selecting all pixels in the Eps-neighborhoods of all non-noise pixels.

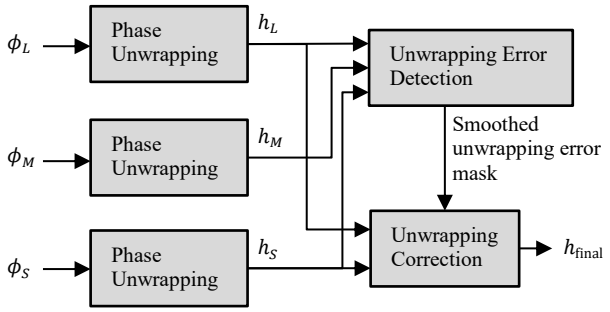

Figure 2 Block diagram of the phase unwrapping scheme with unwrapping error correction. ϕ_L, ϕ_M, and ϕ_S are, respectively, the phases of the large-baseline, medium-baseline, and small-baseline interferograms.

The main challenge of this concept is that CubeSats are characterized by smaller antennas and therefore lower receive gains, which leads to lower signal-to-noise ratio (SNR), and wider antenna patterns, which cause elevated range and azimuth ambiguities. The elevated ambiguities are mitigated by the fact that the antenna pattern on transmit is defined by the antenna of one of the main satellites, which appropriately illuminates the scene. As an example, considering the antennas of the main satellites to be planar with the same size as those of TanDEM-X, i.e., with length of 4.8 m and height of 0.7 m, and the antennas of the CubeSats to be planar with length 0.5 m and height 0.5 m, the receive and two-way antenna patterns are as shown in Figure 3. Similar results would be of course obtained if the CubeSat antenna is a reflector of equivalent size. The receive pattern of the CubeSats is very wide, but the two-way pattern offers some ambiguity suppression, thanks to the the transmit pattern of the main satellite. Considering also the pulse repetition frequency (PRF) to be 3000 Hz and the processed Doppler bandwidth to be 2750 Hz, the resulting azimuth-ambiguity-to-signal ratio (AASR) and range-ambiguity-to-signal ratio (RASR) are, respectively, −17.4 dB and −24.9 dB for the images acquired by the main satellites, and −8.1 dB and −26.2 dB for the images acquired by the CubeSats. Furthermore, Figure 4 shows the effect of the lower receive gain on the SNR decorrelation of the interferograms formed with CubeSat images. There is less SNR decorrelation on the small-baseline interferogram in the first configuration because one of the images used for the interferogram is the image from one of the main satellites, which has a higher SNR compared to the CubeSat. Finally, the small-baseline interferogram has a lower spectral shift decorrelation and lower volumetric decorrelation than the large-baseline one.

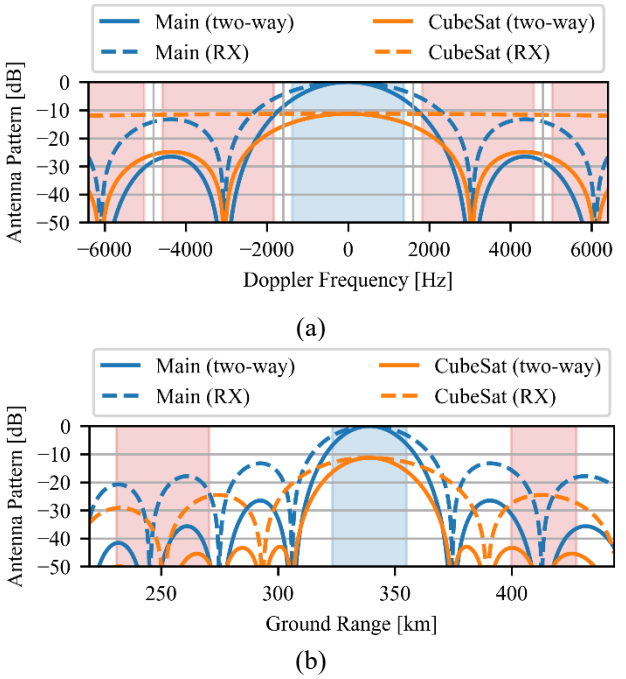

Figure 3 Example two-way antenna patterns for the primary satellite and the CubeSat add-on along (a) azimuth and (b) elevation. The blue and red shaded intervals are, in (a), the processed and ambiguous bandwidths, and, in (b), the main and ambiguous swaths, respectively.

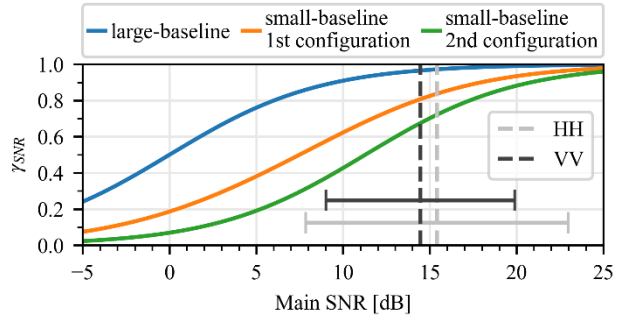

Figure 4 SNR decorrelation of (blue) the large-baseline interferogram and (orange, green) the small-baseline interferogram for each of the two configurations show in Figure 1 as a function of the SNR of the main satellites. The vertical dashed lines and associated error bars mark the SNR in the images of the main satellites corresponding to the mean and 90% occurrence interval of the backscatter from soil and rock at X-band on an incidence angle of 36° for the HH and VV polarizations according to the model from [10].

The probability of occurrence of residual unwrapping errors after the correction (2) serves as a metric for the performance of the CubeSat add-on and it can be evaluated as a function of the coherences, heights of ambiguity, and number of looks of the large-baseline and small-baseline interferograms under the assumption that both are unbiased. The coherence of the small-baseline interferogram can in turn be computed as a function of the size of the CubeSat antenna and the coherence of the large-baseline interferogram. Figure 5 shows the probability of residual unwrapping error as a function of the number of looks in

the small-baseline interferogram and the antenna area of the CubeSat where it has a rectangular antenna and is added in the first configuration, shown in Figure 1 (a), to TanDEM-X-like system, indicating that, with 49 looks in the small-baseline interferogram and a coherence of 0.8 in the large-baseline interferogram, an antenna of 0.25 m^2 would lead to 0.3% probability of residual unwrapping errors, i.e., on average, only 0.3% of the pixels would contain unwrapping errors in the final DEM.

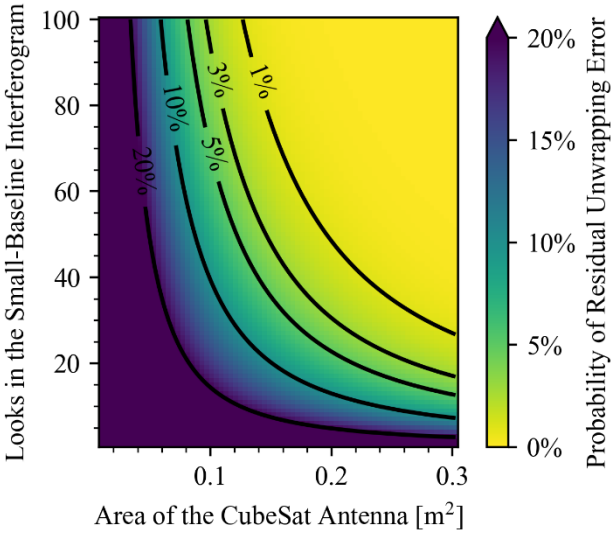

Figure 5 Probability of residual unwrapping error as a function of the area of the rectangular CubeSat antenna and the number of looks used in the small-baseline interferogram. A TanDEM-X-like system is assumed for the main satellites, with a large-baseline interferogram with coherence of 0.8, a height of ambiguity of 20 m, and 25 looks. The CubeSat add-on is assumed in the first configuration, shown in Figure 1 (a), with a small-baseline interferogram with a height of ambiguity of 70 m.

3 Design Example

A design example based on a TanDEM-X-like bistatic interferometer with a CubeSat add-on in the first configuration, shown in Figure 1 (a), is presented to demonstrate and analyze the phase unwrapping correction capability brought by the proposed concept. The analysis uses as input the coregistered pair of images from a TanDEM-X acquisition over an area southwest of Rosenheim, Germany (cf. Figure 6 (a)). From them, estimates of the backscatter, interferometric coherence (cf. Figure 6 (b)) and terrain height across the scene are computed and used to simulate the focused SAR images of the three satellites in the example system over the same scene and with the same incidence angle, but with different baselines. The simulated heights of ambiguity are 20 m, 28 m, and 70 m for the large-, medium-, and small-baseline interferograms, respectively. Note that the height of ambiguity of the large-baseline interferogram is much smaller than the typical height of ambiguity of 30 to 35 m for TanDEM-X [7]. This improves the precision of the final DEM and is possible because the drawback of increased likelihood of unwrapping errors is resolved by the CubeSat add-on. The simulation also includes the two first-order azimuth ambiguities, obtained by shifting the images along azimuth and scaling them according to the expected AASRs, which are −20.5 dB and −12.1 dB for the main and the CubeSat images, respectively.

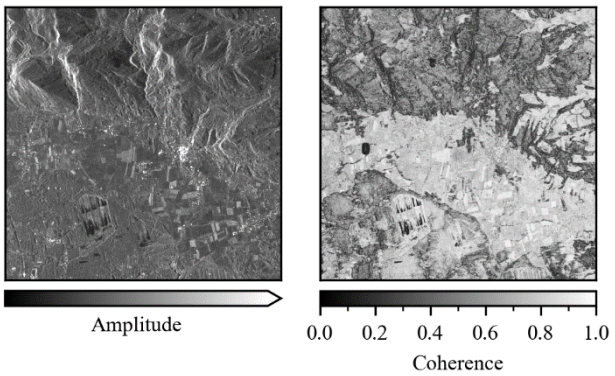

Figure 6 (a) image and (b) interferometric coherence from the TanDEM-X acquisition over an area southwest of Rosenheim, Germany used as input for the simulation.

The simulated images are combined to form the large-, medium-, and small-baseline interferograms, which are then multilooked by averaging over moving boxcar windows of 5 by 5 pixels and 7 by 7 pixels for the large-baseline and the medium- and small-baseline ones, respectively. Figure 7 shows these multilooked interferograms and Figure 8 shows their coherences estimated over the same windows as used for the multilooking.

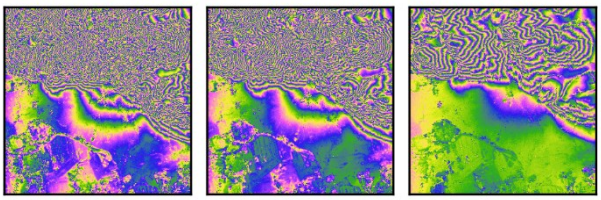

Figure 7 Simulated interferograms for the (left) large-, (center) medium-, and (right) small-baseline interferograms after multilooking.

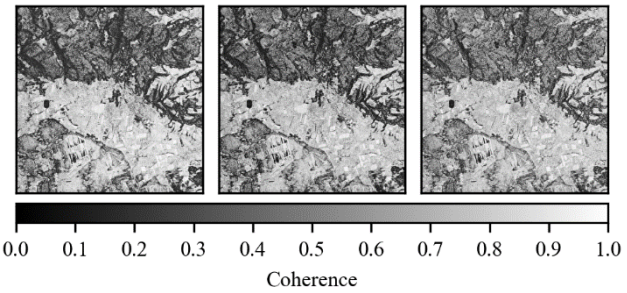

Figure 8 Estimated coherence of the (left) large-, (center) medium-, and (right) small-baseline interferograms shown in Figure 7.

The interferograms are unwrapped, and the resulting large- and small-baseline DEMs are shown in Figure 9. Many unwrapping errors are present in the large-baseline DEM in the mountainous region as evidenced by the various discontinuities indicated by the yellow arrows in Figure 9 (a) and the large height errors shown in Figure 10 (a). The small-baseline DEM, on the other hand, is robust to unwrapping errors, but appears as much noisier, due to its large height variance. The large-baseline DEM is compared to the medium- and small-baseline DEMs to detect phase unwrapping errors, and the resulting mask of detections is smoothed by executing the DBSCAN algorithm [9] with 8 as the minimum number of neighbors and with Eps-neighborhoods defined by a radius of 5 pixels under the Manhattan metric, and then selecting all pixels in the Eps-neighborhoods of all non-noise pixels. The smoothed mask of detections is shown in Figure 10 (b) and includes 99.98% of the pixels with unwrapping errors. On the areas indicated by this mask, the small-baseline DEM is used as a reference to correct the unwrapping errors in the large-baseline DEM through (2), resulting in the final DEM shown in Figure 11. The residual unwrapping errors present in it are shown in Figure 12. They generally occur on areas with very low coherence, such as the edge of forests or the foreshortening areas on the mountainous region. Only 0.26% of the pixels with coherence estimated in the large-baseline interferogram larger than 0.4 contain residual unwrapping errors. Conversely, 95% of the pixels with residual unwrapping errors have a coherence estimated in the large-baseline interferogram smaller than 0.4. Overall, the proposed phase unwrapping correction scheme resolved 93% of the unwrapping errors present in the large-baseline DEM and 81% of the ones not resolved were partially resolved, i.e., had the height error reduced by the unwrapping correction.

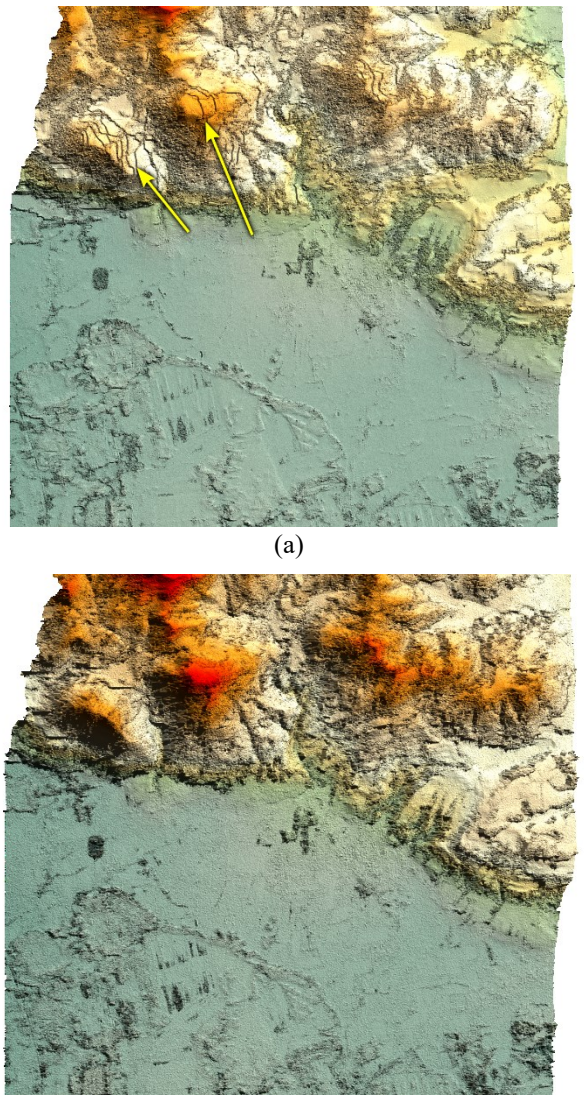

(a)

(b)

Figure 9 DEMs obtained by unwrapping the (a) large-baseline and (b) small-baseline simulated interferograms after multilooking shown in Figure 7. The yellow arrows in the large-baseline DEM point to some of the height discontinuities characteristic of unwrapping errors.

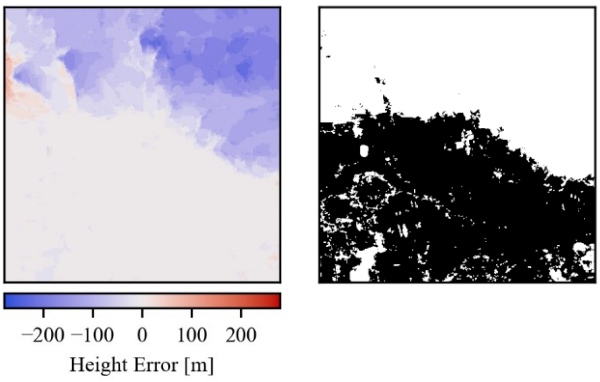

(a) (b)

Figure 10 (a) height error of the large-baseline DEM shown in Figure 9 and (b) the mask, shown in white, of unwrapping errors obtained by comparing the heights of large-baseline DEM with the medium- and small-baseline DEMs.

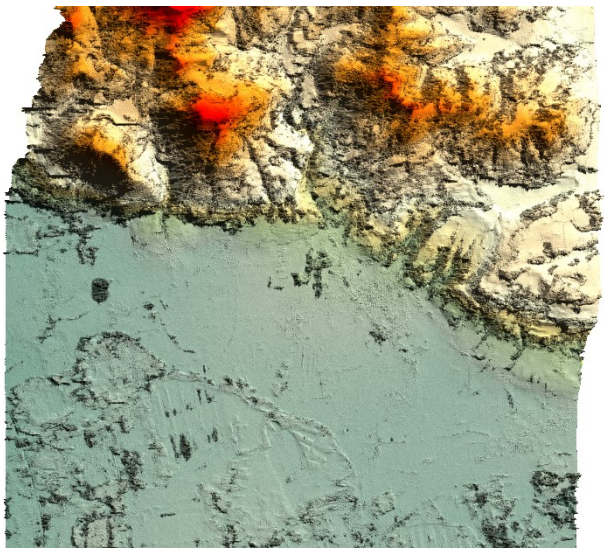

Figure 11 Final DEM obtained by using the small-baseline DEM shown in Figure 9 (b) as a reference to correct the unwrapping errors in the large-baseline DEM shown in Figure 9 (a) through (2) in the areas indicated by the mask shown in Figure 10 (b).

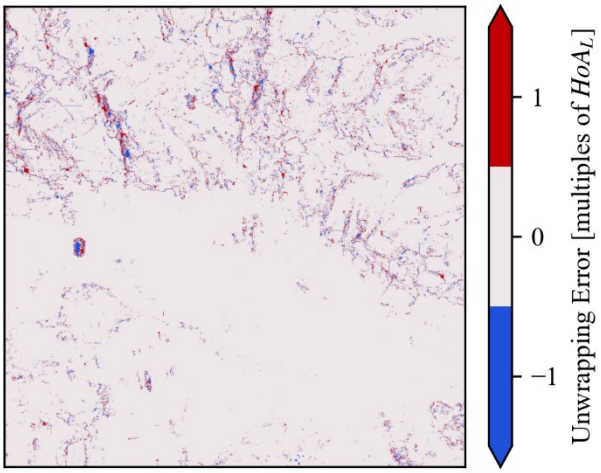

Figure 12 Residual unwrapping errors in the final DEM shown in Figure 11.

4 Conclusion

A CubeSat add-on to bistatic interferometry for detecting and correcting phase unwrapping errors in a single pass of the formation is proposed and analyzed. The concept enables the capability of monitoring fast-changing dynamic phenomena, which is limited in the dual-pass approach employed by TanDEM-X. A design example shows that, even having a lower coherence (due to the much smaller aperture), the additional interferograms, which use the CubeSat add-on data, are effective to correct phase unwrapping errors in the bistatic interferometer through the use of a phase unwrapping algorithm based on the one used in TanDEM-X for combining two passes [7] with key modifications that improve its performance. With the proposed concept, residual unwrapping errors are mostly only present in areas with very low coherence.

The CubeSat add-on therefore allows obtaining accurate digital elevation models, free of phase unwrapping errors, in a single pass of the satellites and paves the way to distributed interferometric systems using clusters of CubeSats.

5 Literature

[1] R. Bamler and P. Hartl, “Synthetic aperture radar interferometry,” *Inv. Probl.*, vol. 14, no. 4, pp. R1–R54, Feb. 1998.

[2] P. A. Rosen et al., “Synthetic aperture radar interferometry,” in *Proceedings of the IEEE*, vol. 88, no. 3, pp. 333-382, March 2000.

[3] R. F. Hanssen, *Radar interferometry: data interpretation and error analysis*, Springer, Dordrecht, The Netherlands, 2001.

[4] A. Moreira, P. Prats-Iraola, M. Younis, G. Krieger, I. Hajnsek and K. P. Papathanassiou, “A tutorial on synthetic aperture radar,” in *IEEE Geoscience and Remote Sensing Magazine*, vol. 1, no. 1, pp. 6-43, March 2013.

[5] Farr, T. G., et al. (2007), The Shuttle Radar Topography Mission, Rev. Geophys., 45, RG2004, doi:10.1029/2005RG000183.

[6] G. Krieger et al., "TanDEM-X: A Satellite Formation for High-Resolution SAR Interferometry," in *IEEE Transactions on Geoscience and Remote Sensing*, vol. 45, no. 11, pp. 3317-3341, Nov. 2007, doi: 10.1109/TGRS.2007.900693.

[7] M. Lachaise, T. Fritz and R. Bamler, "The Dual-Baseline Phase Unwrapping Correction Framework for the TanDEM-X Mission Part 1: Theoretical Description and Algorithms," in *IEEE Transactions on Geoscience and Remote Sensing*, vol. 56, no. 2, pp. 780-798, Feb. 2018, doi: 10.1109/TGRS.2017.2754923.

[8] M. Villano and G. Krieger, "Impact of Azimuth Ambiguities on Interferometric Performance," in *IEEE Geoscience and Remote Sensing Letters*, vol. 9, no. 5, pp. 896-900, Sept. 2012, doi: 10.1109/LGRS.2012.2187271.

[9] M. Ester and H. Kriegel and J. Sander and X. Xu, “A density-based algorithm for discovering clusters in large spatial databases with noise”, in *Proc. KDD*, pp. 226-231, 1996.

[10] F. T. Ulaby and M. C. Dobson, Handbook of Radar Scattering Statistics for Terrain, Artech, 2019.